Rheological evaluation of complex fluids using ultrasonic spinning rheometry in an open container

Taiki Yoshida, Yuji Tasaka, and Yuichi Murai

Citation: Journal of Rheology **61**, 537 (2017); doi: 10.1122/1.4980852
View online: http://dx.doi.org/10.1122/1.4980852
View Table of Contents: http://sor.scitation.org/toc/jor/61/3
Published by the The Society of Rheology

Rheological evaluation of complex fluids using ultrasonic spinning rheometry in an open container

Taiki Yoshida, Yuji Tasaka,[a] and Yuichi Murai

Faculty of Engineering, Hokkaido University, N13W8, Sapporo 060-8628, Japan

(Received 7 October 2016; final revision received 24 March 2017; published 20 April 2017)

Abstract

We propose a rheometry using ultrasonic velocity profiling (UVP) that visualizes and evaluates quantitatively opaque complex fluids in a cylindrical open vessel performing unsteady rotation. The methodology termed "ultrasonic spinning rheometry (USR)" is expected to provide details of various rheological properties. In our study of USR applications, an enhancement in measuring some rheological properties was achieved for three different non-Newtonian fluids. For quantitative evaluations, we focused on momentum propagation in unsteady shear flows from an oscillating cylindrical container. In such flows, this propagation is represented in the radial profiles of the phase lag of velocity fluctuations. The phase lag information is obtained by a discrete Fourier transform of the spatio-temporal velocity distributions measured using UVP and indicates that the phase lag changes substantially as rheological properties change in a test fluid. As the primary rheological property, a local effective viscosity that is representative of the Newtonian viscosity in the bulk of a measurement volume is determined using UVP. In addition, the shear stress distribution, yield stress, spatial viscosity profile, and shear modulus are obtained as secondary rheological properties. © *2017 The Society of Rheology*.
[http://dx.doi.org/10.1122/1.4980852]

I. INTRODUCTION

Like two wheels of a bicycle, rheometry together and suitable rheological models have importance in evaluating rheological characteristics in the fields such as polymers, biology, food processing, and dispersion systems. Most fluid materials dealt with in these fields are non-Newtonian having shear-rate-dependent viscosities [1], exhibiting, for example, shear banding [2] and shear history effects [3]. The development of a universal rheometry that can deal with fluids having any rheological property is an ultimate goal of rheology. Conventional spinning rheometers, employing double cylinders, cone and plate, and double disks, are useful in providing details of physical properties such as the apparent viscosity and linear viscoelasticity subject to simplifying assumptions such as Couette flow in a thin test fluid layer. In practice, however, the behavior is not in accord with assumptions, with differences arising between the expected and actual velocity profiles. Measuring rheological properties, therefore, involves numerous factors associated with errors in conventional systems based on measurements of spinning shear flows and torques. This problem is known as the "Couette inverse problem" [4–6]. Furthermore, there are complexities arising from multiphase fluids that have discontinuities associated with their physical properties because the plate separation in conventional measurement systems is narrow [7,8].

To mitigate such problems, an alternative approach to rheometry, termed velocity-profiling rheometry, which measures the velocity profiles directly, has been proposed in the last decade. Various approaches have been used such as ultrasonic velocity profiling (UVP) [9], ultrasonic imaging velocimetry [10], magnetic resonance imaging velocimetry [11,12], particle imaging velocimetry (PIV) [2,13,14], and laser Doppler velocimetry (LDV) [15,16]. Magnetic resonance imaging velocimetry is required for use in very large measurement facilities but is not suitable for unsteady fluid flows. Both PIV and LDV require transparent test fluids whereas most fluids of interest are opaque. If ultrasonic waves can propagate in the fluids, UVP measurements of opaque fluids such as concentrated suspensions are possible and some work involving UVP rheometry has been reported [17–19]. Ouriev and Windhab [18] proposed an in-line UVP-pressure difference (PD) technique, a combination of UVP measurements and PD measurements. This can be used to calculate parameters of rheological models, such as the shear-rate-dependent viscosity, the power law model, and the Herschel–Bulkley model, to give the best profiles representing the measured velocity profiles under measured pressure difference assuming steady flows. A selected rheological model that does not fit the test fluid cannot provide a useful result. Fluids including different ingredients, bubbles, or particles, are examples of this. Derakhshandeh *et al.* [19] adopted UVP for a wide-gap double-cylinder system that was combined with axial torque measurements to evaluate the rheology of fine fiber suspensions. This approach requires selecting a suitable rheology model and hence suffers from the same problems as the in-line UVP-PD method. These methodologies achieve precise estimates of the rheological properties of fluids that obey ordinary rheological models, but they are not useful in evaluating rheological properties of general complex fluids encountered in industry

[a]Author to whom correspondence should be addressed; electronic mail: tasaka@eng.hokudai.ac.jp

and nature that do not obey simple rheological models. Originally, the spatio-temporal velocity fields measured using UVP reflect all rheological properties and provide a rich source of rheological information. Adopting highly sophisticated rheological models for estimations removes the need to evaluate a precise but restricted set of rheological properties.

We proposed a rheometry using UVP for complex fluids in rotating cylindrical systems without requiring an inner cylinder to measure the axial torque. With simple, open cylindrical containers, measurements of a wide range of target properties are possible. Termed ultrasonic spinning rheometry (USR), this approach has been adopted to evaluate the effective viscosity of a bubbly liquid, corresponding to the Newtonian viscosity in the bulk of a measurement volume of UVP containing tiny bubbles [20]. In the analysis, the phase lag in the velocity fluctuations propagating from the oscillating cylinder wall to the inner part of the fluid is related to the local effective viscosity. Shiratori *et al.* [21] proposed a model-free USR for a quantitative evaluation of the shear-rate-dependent viscosity without adopting any rheological model. This was achieved through a combination of UVP and axial torque measurements in a double-cylinder system as a general circular Couette flow. This method was used to evaluate the viscoelastic properties of fluids using the oscillatory motions of the inner cylinder, and the relationship between strain, strain rate, and shear stress representing the properties as a "flow surface" similar to the flow curves representing shear-rate-dependent viscosity [22]. We also developed an ultrasonic visualizer of the rheological characteristics [23]; here the spatio-temporal velocity field of test fluids in an oscillating cylinder are measured using UVP, from which the distributions of velocity, strain rate, and deformation are calculated and thereby provide in an intuitive manner features of the fluid characteristics.

Through a series of studies, our experimental arrangement has progressed toward a universal USR for general complex fluids including multiphase fluids by extracting information embedded in spatio-temporal velocity distributions measured using UVP. USR makes it possible to quantify various properties from a single measurement of the velocity distributions. The velocity distribution measurements are completed within seconds, and USR can be used to evaluate instantaneous rheological properties that can change rapidly with time. The purpose of the present study is to extend the regime of applicability of USR to general complex fluids through sophisticated signal processing. The proposed USR will provide rapid qualitative evaluations of rheological characteristics and quantitative estimates of such properties in local bulk volumes (cylindrical measurement volume of UVP), principally the effective bulk viscosity of complex fluids. To demonstrate USR capabilities, three test fluids are chosen as examples of thixotropic fluids, shear-thinning fluids, and multiphase fluids. The apparatus, theoretical basis, and procedures of USR are detailed in Sec. II. Details of the test fluids are then summarized, followed by an evaluation of the rheological properties of each test fluid.

II. USR

A. Experimental arrangements

Given the setup of the experimental apparatus (Fig. 1), the experiments were conducted in an open vertical rotating cylinder made of acrylic resin with 145-mm inner diameter ($2R$) and 65-mm high, 2-mm thick lateral wall. There is no lid on the cylinder, which is filled with the test fluid, leaving the top surface of the fluid layer free. The cylinder is mounted at the center of a 1000 mm $\times$ 1000 mm water bath to maintain a uniform temperature T_0 and to allow ultrasonic waves to propagate from outside the cylinder. Oscillations of the cylinder are controlled by a stepping motor set for a given oscillation angle Θ and oscillation frequency f. During an oscillation of the cylinder, the velocity distribution of the fluid is measured using UVP. The ultrasonic echoes obtained are processed using an UVP monitor: Model Duo (Met-Flow S.A., Switzerland) to calculate the spatio-temporal velocity distribution. The type of ultrasonic transducer influences the accuracy of the UVP measurement, and selection takes into account the attenuation of the ultrasonic waves in the test fluid media, minimization of the measurement volume, and reduction in the measurement error in accordance with the fundamental understanding of the UVP method (e.g., [9]). To obtain the azimuthal component of velocity, an ultrasonic transducer of resonance frequency 4 MHz and 5 mm effective element diameter was mounted in the chamber at a horizontal displacement Δy from the centerline of the cylinder.

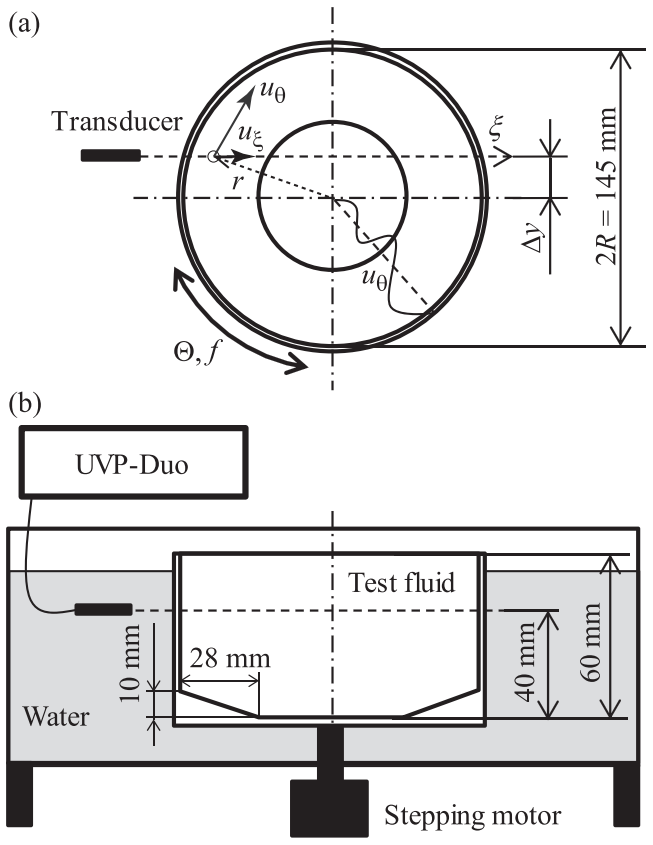

FIG. 1. Schematics of the experimental apparatus for measuring velocity distributions of oscillating shear flows using UVP; (a) top view of the rotating cylinder without the outside container; (b) side view.

The UVP measures the velocity component u_ξ parallel to the measurement line ξ at each measurement point on the line. Assuming that the axisymmetric flow field and the velocity component in the radial direction is negligible compared with the azimuthal component, the azimuthal velocity component u_θ is

$$u_\theta = \frac{u_\xi r}{\Delta y} \tag{1}$$

at a radial position r. Installation of the transducer requires careful handling. Because the measurement volume for UVP is considerable, a much smaller Δy creates significant error and enhances measurement errors. In contrast, larger Δy induces an inflection in the ultrasonic wave at the inner surface of the cylinder wall as a consequence of the large curvature effect. Empirically, based on the results of previous studies [20,23], $\Delta y = 15$ mm was selected. The distance to the wall also needs the proper setting to avoid influences of partially reflected ultrasonic waves at the outer surface of the cylinder. The distance, therefore, was adjusted by monitoring the ultrasonic echo in an oscilloscope experiment. The transducer was set at 40 mm from the bottom of the cylinder to avoid effects of shear stress caused by oscillations at the cylinder bottom plate. The bottom of the cylinder has an axisymmetric down slope running from the cylinder wall to the center (Fig. 1) to suppress the generation of meridional secondary circulations, which induce a considerably large radial velocity component. Suppressing the radial flow requires special attention to ensure the quality of the profiles of the azimuthal velocity component.

The range of applicability of USR is determined by that of UVP, and thus cases of very viscous fluids, for example, larger than 100 000 cSt, and highly concentrated multiphase media would be outside this range because the attenuation of ultrasonic waves in the media is appreciable.

B. Theoretical basis for USR

With this methodology, rheological properties, such as the local Newtonian viscosity, shear stress distribution, and shear modulus, are evaluated quantitatively by comparing the phase lag between the analytical solution and the experimental results. For a comparison of the experimental results of the characteristics of momentum propagation, Tasaka *et al.* [20] derived an analytical solution for the spatio-temporal velocity distribution of Newtonian fluids. When an axisymmetric flow field and a unidirectional flow in the azimuthal direction are assumed, the Navier–Stokes equation for incompressible fluids reduce to

$$\frac{\partial u_\theta}{\partial t} = \nu\left(\frac{\partial^2 u_\theta}{\partial r^2} + \frac{1}{r}\frac{\partial u_\theta}{\partial r} - \frac{u_\theta}{r^2}\right), \tag{2}$$

where ν is the kinematic viscosity of the fluid. Given the initial condition, $u_\theta(r, t=0) = 0$, and boundary conditions, $u_\theta(r=R, t) = U_{\text{wall}} \sin \omega t$ and $u_\theta(r=0, t) = 0$, an analytical solution is found, where $\omega = 2\pi f$ and $U_{\text{wall}} = 2\pi^2 f R\Theta/180$. Further details of the derivation are given in [20].

Here, to confirm the applicability of the analytical solution in the analysis of the experimental data, the azimuthal velocity distribution of silicon oil was measured; this test fluid is typical Newtonian fluids. Figure 2 shows a plot of the radial variation of the phase difference ϕ against the cylinder wall comparing the analytical solution and the experimental results for silicon oil with $\nu = 300\,\text{mm}^2/\text{s}$, $f = 1.0$ Hz and $\Theta = 80°$. In this figure, the radial position is normalized by the radius of the cylindrical container, R. The corresponding analytical solution is given as

$$u_\theta = U_{\text{wall}} A(r) \sin[\omega t + \phi(r)], \tag{3}$$

$$\phi(r) = \tan^{-1}\frac{\Phi_R \Psi(r) - \Phi(r)\Psi_R}{\Phi(r)\Phi_R + \Psi(r)\Psi_R}, \tag{4}$$

by Tasaka *et al.* [20]. The Φ_R, $\Phi(r)$, Ψ_R, and $\Psi(r)$ terms are terms of an infinite series. The phase difference $\phi(r)$ of the experimental data is obtained from a 100 s time series of the instantaneous velocity profiles via a discrete Fourier transformation as the phase of the most dominant frequency component in the power spectrum. The experimental result is in good agreement with the analytical solution for this Newtonian fluid, therefore, the analytical solution may be adequate in describing unsteady flows in the present system. There is considerable, systematic deviation between experimental and theoretical results near the cylinder center in the range, $r/R < 0.3$. This is because the size of the flow circulation compared with the measurement volume: Near the center of the rotating cylinder, the flow changes its direction over a short distance and this influence becomes considerable compared with the measurement volume of UVP.

C. Procedure for evaluating rheological properties

For a quantitative evaluation of general complex fluids, an algorithm for the inverse problem is established using details of the velocity fluctuations obtained in unsteady shear flows. A schematic of the procedure for distinguishing rheological

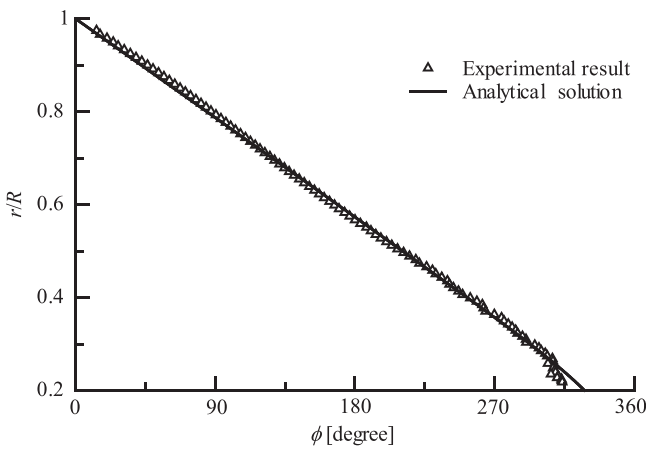

FIG. 2. Comparison of the radial variation in phase difference along the cylinder wall between experimental for silicon oil (kinematic viscosity 300 cSt, oscillating frequency $f = 1.0$ Hz, oscillation amplitude $\Theta = 80°$, temperature $T_0 = 25\,°\text{C}$) and the analytical solution with $\nu = 300\,\text{mm}^2/\text{s}$.

properties is summarized in Fig. 3. Here, we use the phase lag from the cylinder wall calculated using the discrete Fourier transform (DFT) analysis on the spatio-temporal velocity distribution of unsteady shear flows measured using UVP. This provides some advantages in the analysis as summarized below.

First, this analysis can be applied to results with an oscillation period as short as 1 s, which is typical with time resolutions of 25 ms and an oscillation frequency $f = 1.0$ Hz. It is possible to track large changes in instantaneous viscosity as for shear thinning fluids or Bingham fluids. In addition, the influence of measurement noise can be reduced using phase information calculated from the frequency analysis instead of using the spatio-temporal velocity distribution directly: Spikelike noise which is typical of UVP measurements can be removed with the Fourier transform procedure to obtain the local phase difference. Even with the phase information, long-duration measurements may be useful in ensuring a robust estimation of the viscosity of fluids that have constant or slowing-varying viscosity values under the applied shear stress. This enables adjustments in setting optimum measurement times for estimates of a wide range of fluids.

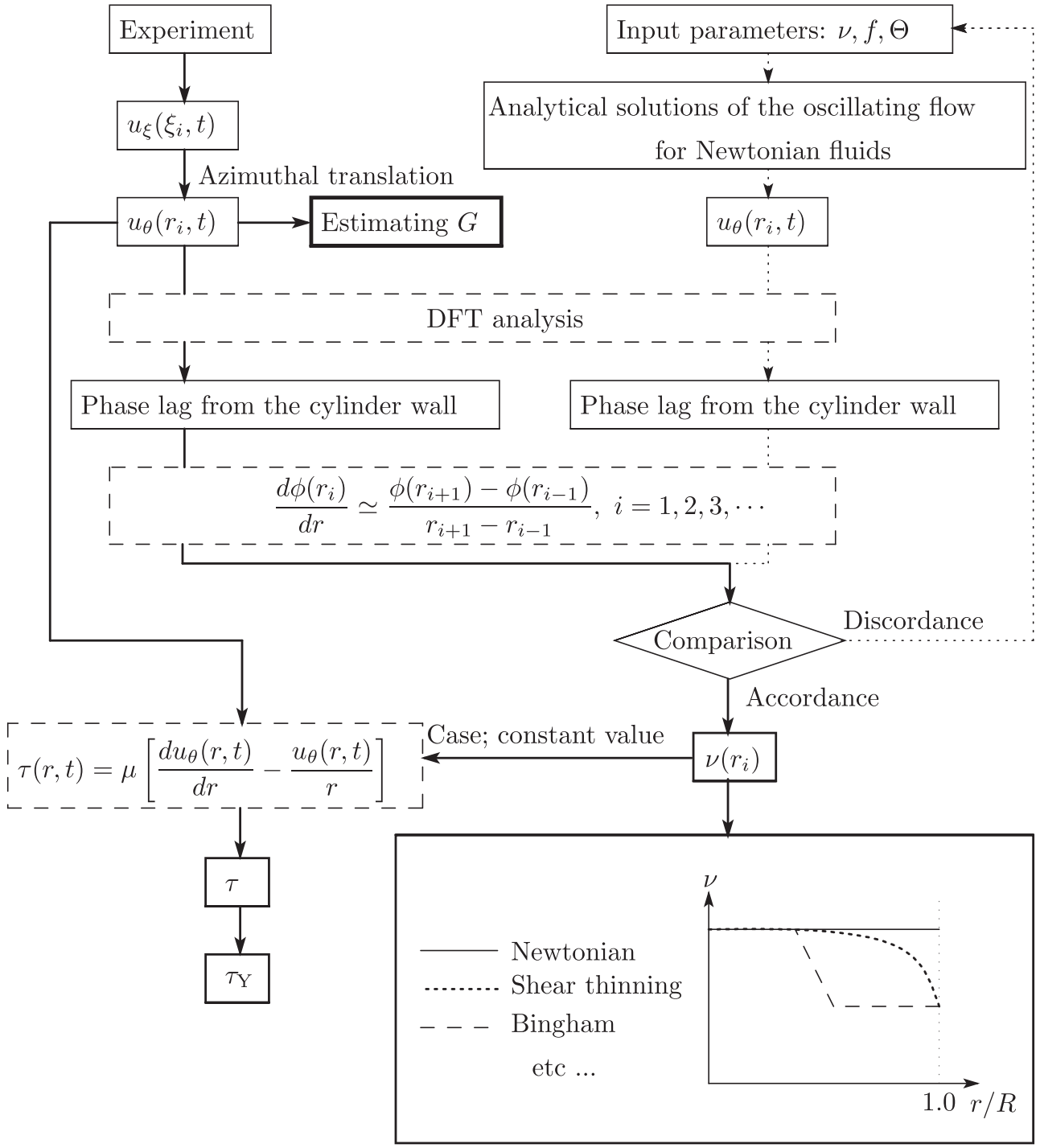

FIG. 3. Schematic outline of the analysis process of USR to evaluate the "local" Newtonian viscosity.

Second, the radial profile of the phase lag can be used to distinguish the rheological characteristics of test fluids: Constant phase lag regimes correspond to rigid rotation and such regimes may be regarded to occur with fluids having elastic properties or very high viscosity values. Regimes with a changing phase lag indicate fluidization areas and thereby can be regarded as fluids with viscous or viscoelastic properties. For example, radial profiles showing a discontinuous variation indicate the existence of boundaries between different regimes of a rheological property.

Finally, the analysis is able to evaluate viscosity values from the gradient of the phase lag, because phase lag represents momentum propagation reflecting viscosity values. By comparing the phase lags of the experimental results with results obtained from the analytical solution, it is possible to evaluate spatial viscosity profiles. Profiles of constant viscosity values indicate that the test fluid is a pure Newtonian viscous body, and therefore, the shear stress distributions $\tau(r)$ can be derived according to Newton's law of viscosity.

Different spatio-temporal velocity distributions contain information representing rheological characteristics other than just the phase difference. As an example of an application of such distributions, a methodology for estimating the shear modulus in elastic deformations G is demonstrated below to show the potential of USR.

III. DEMONSTRATION OF THE POTENTIAL OF SPINNING RHEOMETRY WHEN APPLIED TO COMPLEX FLUIDS

In this section, we discuss the applicability of USR in evaluations of rheological properties through demonstrations of three test fluids with different rheological properties.

A. Test fluids

To emphasize the range of application of our method, montmorillonite suspensions, a fluid food (low methyl pectin gel: LM-pectin gel), and a curry paste containing dispersed solid ingredients were chosen as test fluids. These are, respectively, examples of thixotropic fluids, shear thinning fluids, and fluids with relatively large ingredients. This section describes in detail the rheological characteristics of each fluid.

Montmorillonite is a clay mineral; Fig. 4 shows a schematic of a montmorillonite particle and the structures presented by the particles in a solvent. The particles are polygonal platelets

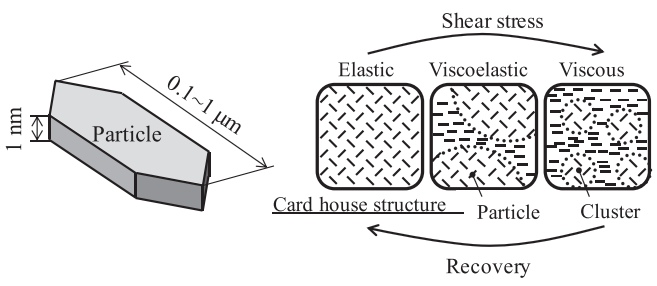

FIG. 4. Schematics of a montmorillonite particle and the breakdown process of its thixotropic structures.

nanometer thickness extending 0.1–1 μm in width. When these particles are dispersed in ionic water, the suspension is a structurally stable through by interactions that has been termed a "Card house structure," as suggested in Fig. 4 (right). This structure however is easily broken into smaller clusters under very weak shear stresses. If still standing in suspension, the structure restores itself with a recovery time t_{rec}. Hence, this complex behavior of the suspension, specifically, time-dependent gelling and high-shear thinning [24] in termed thixotropy. As yet, no measurement system has been established to quantitatively evaluate these behaviors of such suspensions. However, they have been estimated from results attained in various previous investigations [25–27]. In particular, montmorillonite suspensions undergo significant changes in rheological behavior through unsteady shear stresses like those occurring in Bingham fluids, including time-dependent recovery. This describes the qualitative characteristic of the fluid behavior as complex characteristics in determining the rheological properties. Establishment of quantitative details of the rheology of this thixotropic fluid demonstrates the robustness in using USR here. A montmorillonite suspension was prepared by adding 4.0 wt. % powder to 0.01 mol/l NaCl aqueous solutions. (The rheological properties of the suspensions strongly depend on this added volume in addition to the powder concentration.) For full swelling of the particles, the suspension was left for one day before measurements were taken. After filling the cylinder, the suspension was stirred vigorously to eliminate any shear stress history.

The second test fluid, LM pectin gel is a dessert base (Fruiche, House Foods Group, Inc.). This has a gelling action arising from the interaction between Ca^{2+} inside the milk and the chain structure of the LM-pectin polymers. In the food industry, this interaction has been used to thicken fluid foods forming complicated entangling clusters causing an egg-carton-shaped structure (Fig. 5). An exerted momentum, for example, from shear stress, reduces the cluster size caused by suppressing the interactions between polymers. Thus, the LM-pectin mixture exhibits a shear thinning [28]. Such fluid foods display a stronger viscoelastic behavior than montmorillonite suspensions. When the fluid food propagates a momentumlike shear stress or by stirring, it exhibits both springlike and dashpotlike characteristics. In this experiment, we prepared the fluid food following a published recipe (House Foods Group Inc. recipe): (200 ml milk for each 50 mg of powder; the specifications of the milk used are 85 mg Na, 227 mg Ca, and 6.5 g protein in 200 ml). This fluid includes a lot of fruit pulp, which has formless shape and deforms under shear stress. Thus, this fluid features boundaries

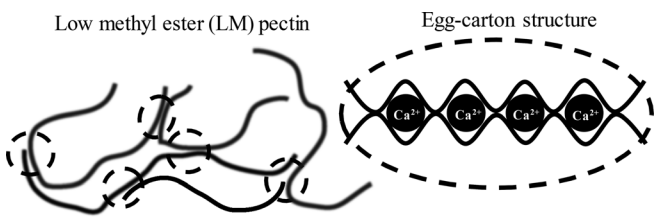

FIG. 5. Schematics of LM-pectin cluster and the egg-carton structure.

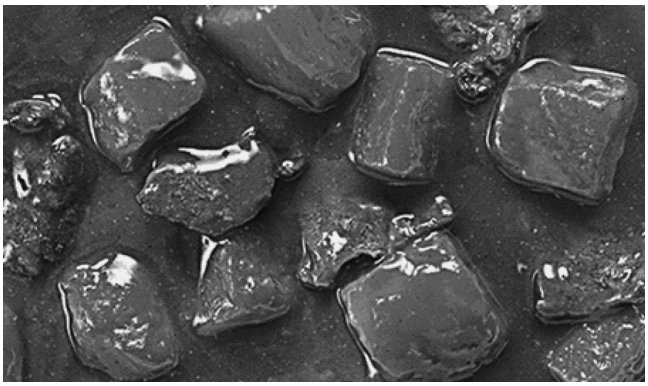

FIG. 6. Photo of curry paste containing dispersed ingredients.

in its distributions in physical properties arising from shear deformation.

The third test fluid is a curry paste, which is a commonly consumed fluid food containing relatively large pieces of ingredients. An ordinary retort-pouched curry paste (Bon curry, Otsuka Foods Co.) was chosen. Figure 6 shows that some of the ingredients, such as lumps of fat and spices, are nonuniformly dispersed in the curry paste. In addition, the shapes and sizes of the ingredients are nonuniform. Thus, being highly complex, details of its rheological properties or indeed other liquids containing such ingredients are difficult to obtain. The curry paste includes beef tallow and butter made from milk. The melting point of the beef tallow is around 40 °C and that of the butter 30–40 °C. With low melting points, these fluids result in a decrease in viscosity with increasing temperature. Here, we want to evaluate essentially the effective viscosity of this complex suspension using the proposed rheometry.

B. Results and discussion

The spatio-temporal velocity distributions measured by UVP reflect the rheology of the test fluids, and based on this a qualitative evaluation of the rheology can be obtained from these distributions. Rheological properties were measured and analyzed according to the procedure summarized in Fig. 3. From the analysis, the applicability of the present method to the various types was assessed using the measurement resolutions of the UVP, as specified in Table I. The spatial resolutions specified in the table were determined theoretically from the number of cycles of ultrasonic wave and the speed of sound in the test media. The actual number of waves in a single emission of ultrasonic waves changes depending on the damping quality of the piezoelectric elements in ultrasonic transducers, and usually increases. There is, however, no considerable spatial averaging effect due to larger measurement volume at least in the experiments in this study; for example, see Fig. 1.

TABLE I. Time, velocity, and spatial resolutions in the UVP measurements.

Test fluid	Time (ms)	Velocity (mm/s)	Spatial resolution (mm)
Montmorillonite suspension	25	1.304	0.74
LM-pectin gel	25	1.368	0.75
Curry paste	24	1.563	0.78
Silicon oil (300 mm^2/s)	30	0.664	0.62

1. Montmorillonite suspension

With the montmorillonite suspension, the assumption of axisymmetry and unidirectional flow in the azimuthal direction, the spatio-temporal velocity map obtained by the UVP can be converted into a radial-temporal distribution of the azimuthal velocity component. Figure 7 shows the distribution obtained at different elapsed oscillation times with $f = 1.0$ Hz in the oscillation frequency and $\Theta = 90°$ in amplitude; here the vertical and horizontal axes indicate the radial positions normalized by the radius of the cylindrical container, R, and the spin-cycle time. The gray scale contours represent the azimuthal velocity normalized by the maximum azimuthal velocity at the cylinder wall, U_{wall} $\left(= 2\pi^2 f R\Theta/180\right)$. From these distributions, the oscillation of the azimuthal velocity propagates as a damped wave from the wall to the center of the

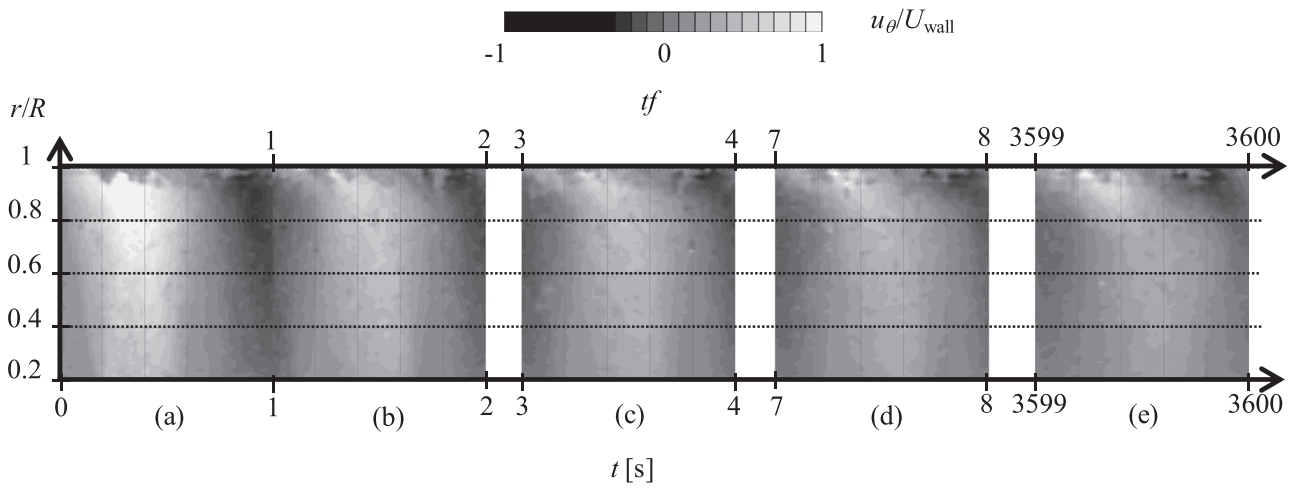

FIG. 7. Azimuthal velocity distributions of the montmorillonite suspension (4.0 wt. % powder to a 0.01 -mol/L NaCl aqueous solution) at different elapsed oscillating time, where the oscillation frequency, amplitude, temperature, and recovery time are $f = 1.0$ Hz, $\Theta = 90°$, $T_0 = 20$ °C, and $t_{\mathrm{rec}} = 100$ min, respectively; $U_{\mathrm{wall}} = 715.5$ mm/s.

cylinder. From Figs. 7(a)–7(e), the phase lag from the cylinder wall to the inner parts of the fluid develops into the inner region of the fluid layer with time. Because the phase lag represents local rheological properties as explained in Sec. II C, this development typifies the thixotropic behaviors of the suspension as the viscosity decreases with applied shear stress. There is a constant phase-lag regime in the inner region of the cylinder, which can be assumed to be an unyielded region maintaining the gel state. The boundary between the yielded and unyielded regions moves gradually toward the center, cycle-by-cycle, and reaches an equilibrium state around $t = 1800$–1900 s [Fig. 7(e)]. To quantify the phase lag, the velocity distributions were analyzed by time-directional DFT for 1 s periods. Figure 8 shows the radial profiles of the phase lag ϕ based on the cylinder wall oscillation at each time-interval section (a)–(e) indicated in Fig. 7.

The phase lag profiles assume almost constant values except near the cylinder wall at the beginning. With increasing oscillation time t, the phase lag becomes larger and the regime with phase lag widens progressively. This indicates that the viscosity of the suspension in the cylinder is decreased by the applied shear stress from the oscillating cylinder. Eventually, the development of the phase lag profiles converges at time section (e), $t \sim 3600$ s from the start of the oscillation of the cylinder. There are two clearly separated yielded and unyielded (fluidized or unfluidized) regions illustrated in Fig. 8 (right). The discontinuity in the curve at which the profiles show a change in the variation (see Fig. 8) indicates the boundary between the yielded and unyielded regions.

In the yielded region for each time step in Fig. 8, the gradient of the phase lag profile remains largely unchanged. This suggests that the fluids in the yielded region have assumed distinct rheological properties. In the figure, the dashed inclined line indicates the phase lag profile obtained from the analytical solution for Newtonian fluids given in Eq. (4). The profile corresponds closely to that at time step (e) within the range $0.75 < r/R < 1.0$, and therefore, the suspension in the yielded region can be assumed to behave as a Newtonian fluid similar to Bingham fluids, which has a yield stress and no viscoelasticity. The least-squares approximation representing the best representation of the experimental profile in the $0.8 < r/R < 1.0$ range provides a corresponding Newtonian viscosity $\mu = 0.489$ Pa s. In a previous study [29], the value of montmorillonite suspensions with the same NaCl percentage as in the present suspension was estimated as 0.528 Pa s using a conventional rheometer. The conventional rheometer has measurement uncertainties in addition to random measurement errors, deriving from the influence of shear banding, slipping at the wall, and other phenomena, whereas the present measurement evaluated the value in the pure Newtonian regime. Considering measurement uncertainties, these values achieve good agreement. Additionally, this shows that the present rheometry using UVP is able to monitor the evolution of yielding from the cylinder wall to the inner region as a typical rheological behavior of the suspension.

Assuming that the suspension in the yielded region is a Newtonian fluid makes it possible to estimate the local shear stress using Newton's law of viscosity

$$\tau(r,t) = \mu\left[\frac{du_\theta(r,t)}{dr} - \frac{u_\theta}{r}\right]. \tag{5}$$

Substituting the analytical solution of Eq. (3) into Eq. (5) provides the shear stress distribution in the yielded region. The maximum value among the radii in the time series is shown in Fig. 9 as a dashed curve. Also, plotted for comparison are the shear stress values calculated from the experimental results with the numerical derivatives of Eq. (5) obtained using the secondary central difference method. The plots show rather large deviations from the analytical solution near the wall, but further away from the wall the variation follows

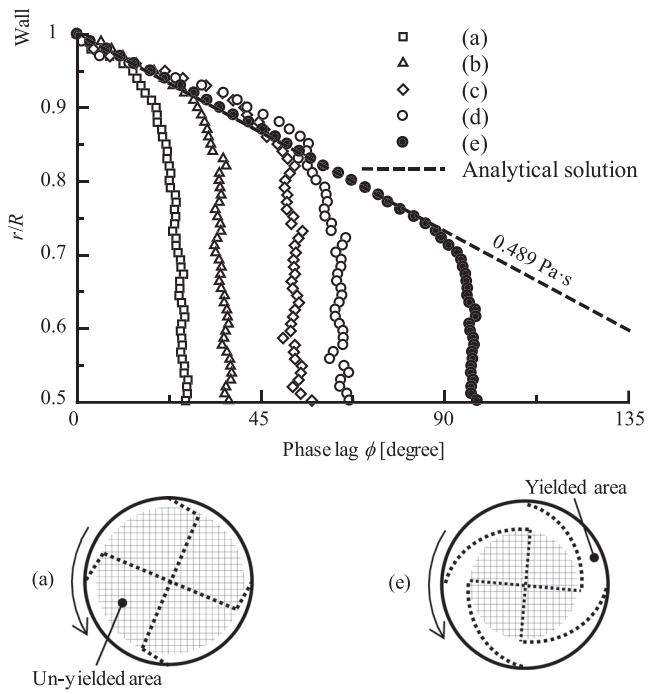

FIG. 8. Phase lag of the local velocity fluctuations from the cylinder wall at each time step (a)–(e) indicated in Fig. 7, and schematic of phase lag.

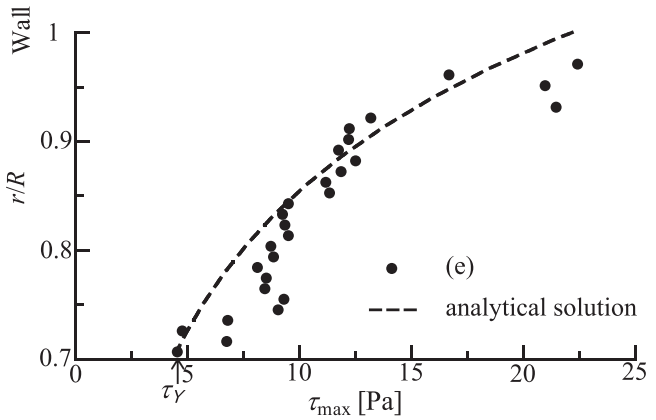

FIG. 9. Radial profile of the local maximum shear stress; the dashed line represents the values calculated from the analytical solution with an estimated viscosity and the data points are from the spatio-temporal velocity distribution shown in Fig. 7(e) using numerical derivatives.

the analytical solution. For the present experimental conditions, the boundary between the yielded and unyielded regions is around $r/R = 0.7$; Fig. 9 implies that the shear stress value at $r/R = 0.7$ is suggestive of a yield stress value $\tau_Y = 4.57$ Pa for the suspension. It is often difficult to evaluate the yield stress value by rheometry using only velocity information, and this result highlights the advantage of the present rheometry.

The original spatio-temporal velocity distributions measured by UVP in the present system provide more information of the rheology than the phase difference extracted from the distributions, whereas the phase difference still provides robust estimates of the viscosity via the analytical solution. As an example of further analysis that is possible from the rheology with the velocity distribution, we next focus on variations in the velocity distribution immediately after the start of the oscillation. In Fig. 7(a), the inner fluid flow is stationary, and the fluid exhibits elastic properties. Immediately after the oscillation starts, there is an elastic wave propagating with velocity v_e. From the elastic-wave theory [30], v_e is given by

$$v_e = \sqrt{\frac{G}{\rho}}, \tag{6}$$

where G and ρ denote shear modulus and density, respectively, with ρ a constant value. As v_e varies proportionally to $G^{1/2}$, this makes it possible to estimate the shear modulus from the azimuthal velocity distributions obtained by UVP. Figure 10 shows the instantaneous radial velocity profiles immediately after the oscillation begins. Here, an initial damped wave propagates from the cylinder wall; its speed can be estimated from the velocity distribution. The front edge of the wave can be estimated by introducing a threshold, in the present case $u_\theta/U_{wall} = 0.1$ was chosen. The speed of the damping wave v_e is obtained from $v_e = \Delta r/\Delta t$ (see Fig. 10). The propagation speed v_e and Eq. (6) provide the shear moduli, G, for different recovery times after stirring, t_{rec}. The logarithmic plot of G versus t_{rec} in Fig. 11 gives the dependence of the shear modulus on recovery time. Rand *et al.* [31] proposed an empirical formula of the recovery time dependence on the shear modulus G given by

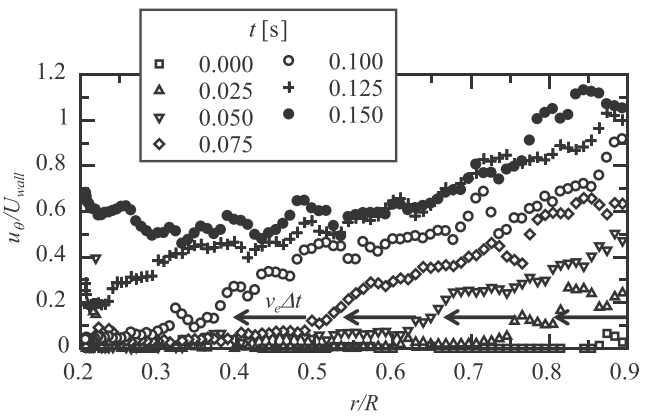

FIG. 10. Initial development of the radial velocity profiles with time increment of 0.025 s for various staring times of the cylinder oscillation extracted from the results for the montmorillonite suspension given in Fig. 7.

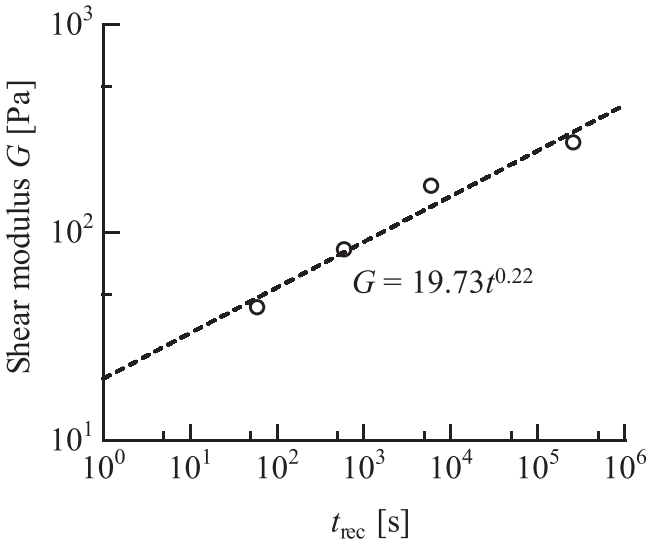

FIG. 11. Shear modulus versus recovery time after stirring.

$$G = G_0\left(\frac{t_{rec}}{t_0}\right)^{\alpha}, \quad t_0 = 1\ [\mathrm{s}]. \tag{7}$$

Here, G_0 and α are the zero shear modulus and a constant exponent, respectively. The results obtained obey this formula and using a least-squares fit on the plot (Fig. 11) provides values of $G_0 = 19.73$ Pa and $\alpha = 0.22$, respectively. These values seem quite reasonable in comparison with the time-dependence of the rheological properties such as the thixotropic behavior.

2. LM-pectin gel

For the LM-pectin gel, Fig. 12 shows the azimuthal velocity distributions of the LM-pectin layer at various elapsed oscillation times measured using UVP. The measurements were performed after leaving the gel at rest for 100 min after mixing. As unidirectional flow can be realized, the parameters of the oscillation were set at $f = 1.0$ Hz and $\Theta = 60°$ in each of the measurements in the test fluids. The oscillation in the azimuthal velocity propagates from the wall to the center of the cylinder as a damped wave. The time development of the velocity distributions is similar to that in the montmorillonite suspension, specifically, the region near the wall with radial variations in the phase lag widens and the boundary of the region has a constant phase lag that moves toward the center. However, the development of the velocity distribution appears to be slower than the montmorillonite suspension. To quantify the development of the phase lag profiles, the phase lags of the velocity distribution were obtained from the DFT analysis detailed in Sec. II C. To obtain a smooth curve for the phase lag, velocity distributions of longer periods of 100 s were used for the analysis. Figure 13 shows examples of the radial phase lag variations obtained at periods, $t = 0$–100 s, $t = 600$–700 s, and $t = 1800$–1900 s.

In the initial period ($t = 0$–100 s), the phase lag has a plateau region at the inner part, and with increasing oscillation time, the curve of the phase lag changes progressively and orderly. In comparison with the results for the montmorillonite

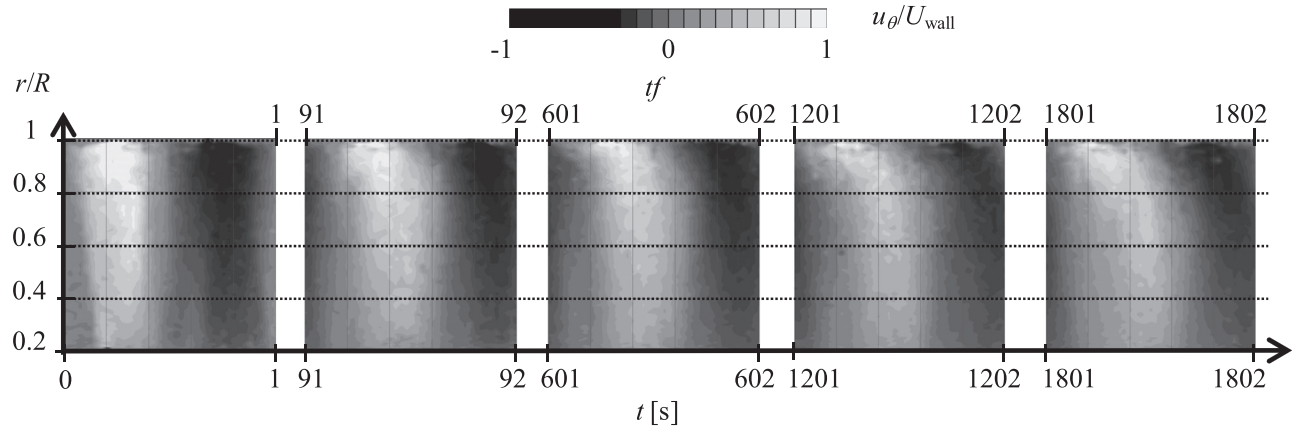

FIG. 12. Azimuthal velocity distributions at each elapsed oscillating time measured using UVP in LM-Pectin gel, where the oscillation frequency, amplitude, and temperature are $f = 1.0$ Hz, $\Theta = 60°$, and $T_0 = 15\,°$C, respectively; $U_{\text{wall}} = 477.0$ mm/s.

suspension (Fig. 8), the phase lag in the profiles in Fig. 12 shows a smoother variation from the cylinder wall to the center of the container, and there is no clear boundary between yielded and unyielded regions. This can be ascribed to changes in the polymer structure in the gel. Polymerization and gelation of fluids provide a shear-dependent viscosity and elastic properties, and the relaxation of the polymer structure and storage of shear stress by elastic effects make the boundary diffuser. Also, the slope of the curve in the yielded region is not constant, but increases over time. This suggests that the rheological properties are not constant in the yielded region and that the effective viscosity decreases with time. The curve plots of the phase lag indicate qualitatively rheological properties like the Herschel–Bulkley viscous suspensions unlike the viscous properties of Bingham plastic such as the montmorillonite suspension. The shape of the profiles does not change from that shown in Fig. 13 at $t = 1800$–1900 s, and it may be assumed that the modification of the polymer structure reaches a terminal state in relation to the shear conditions.

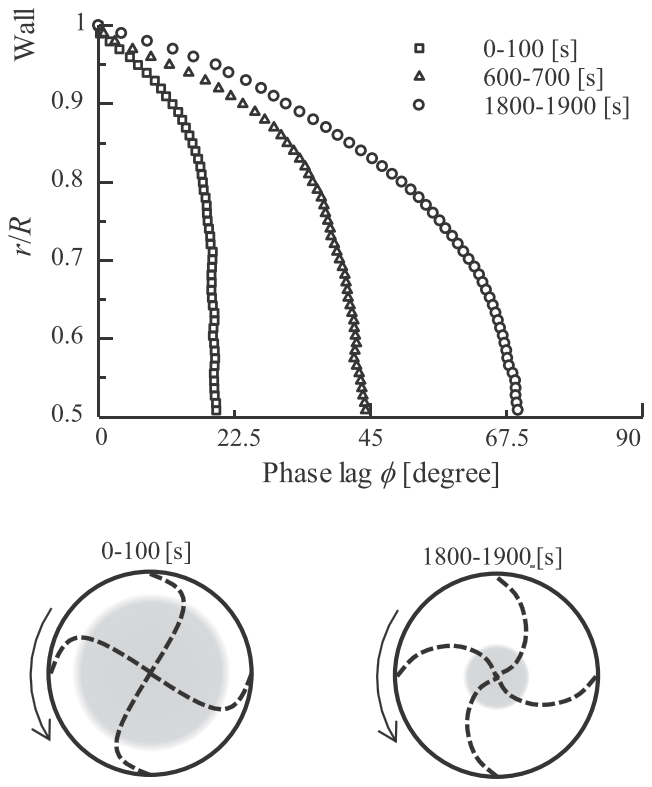

FIG. 13. Phase lag of the local velocity fluctuations from a cylinder wall for different 100 s waiting-time intervals, and schematic of phase lag.

Assuming a fluid of very large viscosity, momentum propagation for unsteady shear flows in a fluid reaches very large speeds. The resultant phase lag has a constant value at each radial position as in rigid rotation. Paradoxically, the resultant phase lags were strongly dependent on the viscosity value of the test gel fluids because the information obtained of the phase lags indicates momentum propagation from the wall to the center. In other words, a decrease in the viscosity value of the test fluid causes an increase in the phase lag. In Fig. 13, changes in the phase lag for different elapsed cycle numbers are indicative of viscosity decreases from the shear stress induced by the oscillation. The gradient of the phase lag profile changes continuously in the radial direction, and this suggests a radial variation in viscosity. Here, the gradient is estimated using the discrete equation of the secondary central difference method

$$\frac{d\phi(r_i)}{dr} \approxeq \frac{\phi(r_{i+1}) - \phi(r_{i-1})}{r_{i+1} - r_{i-1}},\ i = 1, 2, 3, \ldots. \tag{8}$$

Figure 14 displays plots of the gradients in the phase lags of the spatio-temporal velocity distribution taken from the LM-pectin gel measurements; that for the montmorillonite suspension is shown in Fig. 8(e). The dashed lines represent the gradient profiles calculated from the analytical solutions using the Newtonian viscosity for various kinematic viscosities, and these form contour lines of viscosity. The profiles of the gradients show clear tendencies despite deviations arising from higher measurement noise appearing because of the numerical calculation of the derivatives. For the LM-pectin gel, the data points in the first period ($t = 0$–100 s) yield the largest fluctuations among all the data. This is because the viscosity of the test fluid changes considerably immediately after the start of the oscillation from shear thinning effects. The gradient profile for montmorillonite maintains a nearly constant value for $r/R > 0.7$, suggesting that it

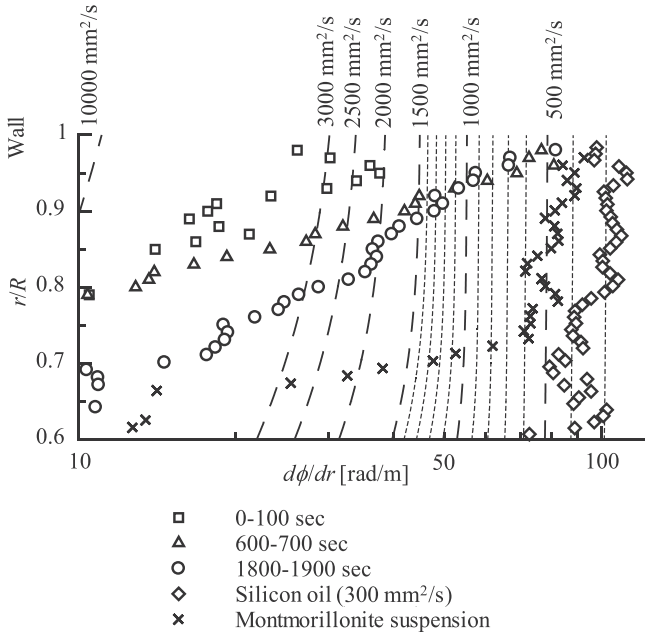

FIG. 14. Gradient of the radial profiles of the phase lag for different elapsed time, where contour lines represent results from the analytical solution for various kinematic viscosities.

behaves like a Newtonian fluid in this region. The following sharp drop in the gradient around $r/R = 0.7$ indicates that there is a buffer region between the Newtonian-like fluid and the unyielded regions as noted in Sec. III B 1. The local gradient of the phase lag has a corresponding Newtonian viscosity, and therefore, it is possible to determine local effective viscosities which reflect all of the viscoelastic effects as Newtonian viscosity. The effective viscosity is determined from the local crossing points of the gradient profiles with the contour lines of the corresponding viscosities.

Figure 15 shows results of the spatial viscosity analysis for each profile of the phase gradient (shown in Fig. 14); only the $0.8 < r/R < 0.95$ range is shown for clarity. These plots for the first period of the LM-pectin ($t = 0$–100 s) have larger viscosities at all radial positions than at the following periods, $t = 600$–700 s and $t = 1800$–1900 s. In the second period, the viscosity is small near the cylinder wall and increases toward the inside of the cylinder. The plot of the third period ($t = 1800$–1900 s) shows a more gradual increase in the viscosity than at earlier periods and takes similar values as the second period near the cylinder wall: Here, the viscosity appears to converge to the lower limit of the viscosity. Decreases in the viscosity are caused by fragmentation of the clusters in the LM-pectin gel, and therefore, the smallest viscosity around 1000 mm^2/s may correspond to the limit of the breakup because of the applied shear stress at the wall. Different from the LM-pectin gel, the plots for the montmorillonite suspension assume an almost constant viscosity around 470 mm^2/s (corresponding to 0.489 Pa s) at all radial positions. This result indicates that the particle clusters in the suspension are fully fragmented in this radial range, and hence the suspension may be considered to behave as a pure (uniform) viscous fluid. In addition to these results, the kinematic viscosity of silicon oil (300 mm^2/s at 25 °C; see corresponding phase-lag profile in Fig. 2), which is a Newtonian fluid, was evaluated to be near 300 mm^2/s. This provides supporting evidence of the measurement precision of the present estimation procedure; within 5% accuracy assuming 300 mm^2/s is the true value with no deviation.

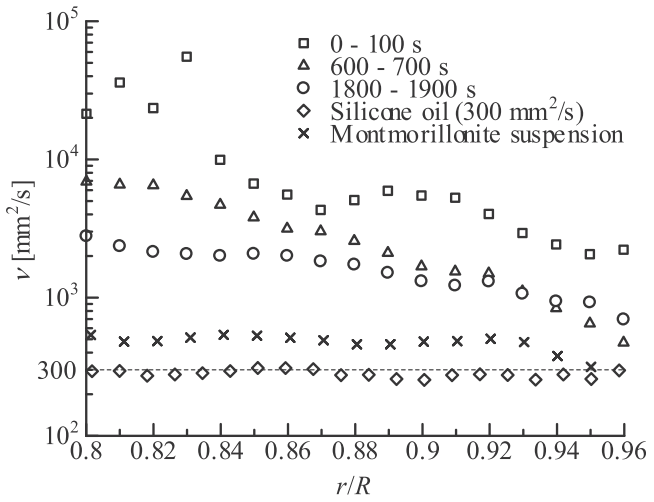

FIG. 15. Local effective viscosity distributions of LM-pectin gel at each elapsed time and the distributions of montmorillonite suspension and 300 mm^2/s silicone oil.

3. Curry paste with dispersed ingredients

Figure 16 shows the azimuthal velocity distributions of curry paste in cylindrical unsteady shear flow with an oscillation frequency $f = 2.0$ Hz and amplitude $\Theta = 45°$ obtained for two temperatures $T_0 = 35$ °C (upper panels) and 40 °C (lower panels). Comparing these figures indicates that the spatial velocity distributions are considerably different at $20 < t < 21$ s; the distributions for $T_0 = 40$ °C also change more considerably. To evaluate this change quantitatively, the phase lags of the fluctuation were calculated in a DFT analysis, as in Sec. III B 1. To capture the time development of the phase lag, a 1 s period was chosen for the DFT analysis.

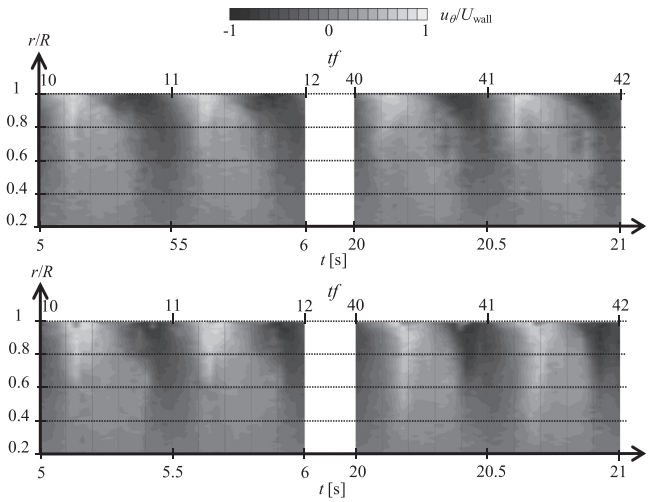

FIG. 16. Azimuthal velocity distributions of the curry paste at each elapsed oscillating time, where the oscillation frequency and amplitude are $f = 2.0$ Hz and $\Theta = 45°$, respectively, setting temperatures are; (upper) $T_0 = 35$ °C, and (lower) $T_0 = 40$ °C; $U_{wall} = 715.5$ mm/s.

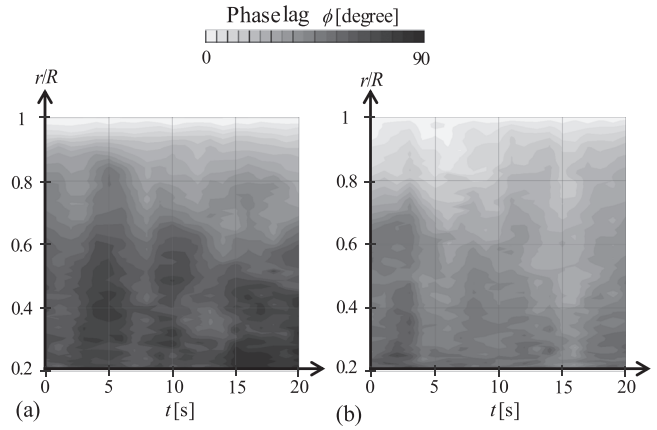

FIG. 17. Radial-time distribution of phase lag in the local velocity fluctuations from a cylinder wall for curry paste at fixed temperatures (a) $T_0 = 35\,^{\circ}\mathrm{C}$, (b) $T_0 = 40\,^{\circ}\mathrm{C}$.

From the time variations in the phase lag profiles for the two preset temperatures (Fig. 17), the phase lag increases with time for the lower temperature, and the variation is more pronounced near the wall as indicated by the distortion in the phase-lag profile. This result arises most likely because of the shear thinning viscous behavior in rheological properties of curry paste due to the solid clusters of beef tallow and other ingredients. For the higher temperature, the phase-lag variation is more gradual. Generally, the viscosity of fluids decreases with increasing temperature. However, this result indicates the contrary, with an increase in viscosity with temperature. We infer that this phenomenon occurs because of dilatant behavior from a concentration of ingredients in curry paste. At the lower temperature, the viscous resistance and centrifugal forces on ingredients are balanced. However, because the viscosity of beef tallow decreases with increasing temperature, centrifugal forces exceed the viscous resistance, and this allows the ingredients to move more freely. A slight radial motion of the ingredients may increase momentum propagation from the wall that is reflected in a widening of the area with phase lag. We stress that this phenomenon is correlated with the melting point of beef tallow (almost 40 °C) and butter (30–40 °C) in curry paste.

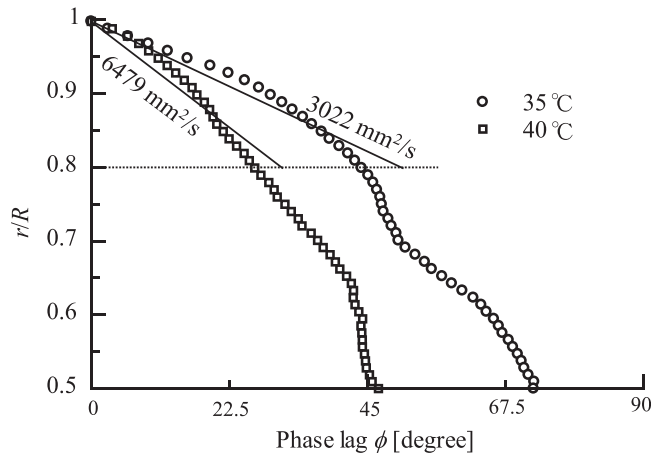

FIG. 18. Phase lag of the local velocity fluctuations from a cylinder wall for curry paste at two fixed temperatures.

To determine quantitative differences in the rheological characteristics between two set temperatures, phase lag profiles (Fig. 18) were obtained from an analysis of all the time profiles (25 s) using the DFT analysis. From their form evaluating the viscosity is difficult as it is influenced by the dispersed multiphase properties in curry paste. By averaging the gradients of the phase lag at each radial position, estimates of the viscosity in the bulk volume can be obtained. From these averaged gradients in the radial range, $r/R = 0.8$–1.0, the values estimated for the viscosity were $3022\,\mathrm{mm}^2/\mathrm{s}$ for $T_0 = 35\,^{\circ}\mathrm{C}$ and $6479\,\mathrm{mm}^2/\mathrm{s}$ for $T_0 = 40\,^{\circ}\mathrm{C}$. These values are effective bulk viscosities for the test fluids plus ingredients, estimated from momentum transfer from the cylinder wall. In brief, the viscosity of beef tallow decreases with increasing temperature that simultaneously allows the ingredients to move more freely in the radial direction. This increases the effective bulk viscosity in the solution estimated with the present USR.

IV. CONCLUSIONS

To provide a visualization and quantitative evaluation of opaque and complex fluids, which are commonly encountered in industry and nature, we have proposed a rheometry using UVP, termed USR, which permit measurements to be taken of fluids in an open cylindrical vessel undergoing unsteady rotation. The USR approach provides a qualitative evaluation of rheological characteristics and a quantitative estimate of rheological properties in the local bulk volume. The principle property is the effective bulk viscosity of general complex fluids using phase-lag information extracted from spatio-temporal velocity data measured by UVP.

Three fluids, montmorillonite suspension, LM-pectin gel, and curry paste, with different complex behaviors were used as test fluids to demonstrate the utility of USR. These test fluids are typical examples of thixotropic fluids, pseudoplastic fluids, and fluids containing large semisolid ingredients. For the montmorillonite suspension, the phase lag appears as its time-dependent viscosity decreases in the suspension through unsteady shear stress induced by oscillations at the cylinder wall. In the yielded region, the radial profile of the phase lag closely follows the analytic solutions for a Newtonian fluid; the corresponding Newtonian viscosity was found to be $\mu = 0.489\,\mathrm{Pa\ s}$ along with a yield stress of $\tau_Y = 4.57\,\mathrm{Pa}$. The local gradients of the phase-lag profiles lead to corresponding viscosities, and this makes it possible to obtain local effective viscosities, which reflect all viscoelastic effects as an effective Newtonian viscosity. The effective viscosity is determined from the local crossing point of the gradient profile with the contour of the corresponding viscosity. For LM-pectin gel, a decrease in the viscosity occurs through the fragmentation of large gel clusters into smaller ones, and the smallest viscosity recorded, of around $1000\,\mathrm{mm}^2/\mathrm{s}$, may correspond to the limit at which clusters break up near the container wall under the applied shear stress. In the determination of the viscosity of curry paste, the viscosity values were estimated at $3022\,\mathrm{mm}^2/\mathrm{s}$ for $T_0 = 35\,^{\circ}\mathrm{C}$ and $6479\,\mathrm{mm}^2/\mathrm{s}$ at $T_0 = 40\,^{\circ}\mathrm{C}$. These values are

effective bulk viscosities of curry paste plus ingredients, estimated from momentum transfer from the cylinder wall.

In summary, USR provides useful rheometry determining instantaneous rheological properties in the local bulk volume (corresponding to the cylindrical measurement volume used for UVP). The measurement of the velocity profiles is completed within seconds and USR is able to capture rheological properties in a run-time manner. Postprocessing to extract useful rheological information offers excellent potential for obtaining details of other rheological properties. Further developments of USR could establish a method for evaluating not only the viscosity but also the elasticity from velocity information something that appears highly attractive. Other options may include methods for measuring viscoelasticity through linear analysis using a rheology model such as the Maxwell model for complex fluids. In performing linear viscoelastic analysis with velocity information only, measurement noise will be a considerable problem to overcome. The development of UVP technology and ultrasonic velocimetry in general also has been progressing. Ultrasonic measurements of velocity fields still have a large potential in resolving and expanding on current information [32–34]. These developments will improve the capability of USR procedures.

ACKNOWLEDGMENT

The authors appreciate fruitful discussions and comments from Professor Peter Fischer, ETH Zürich.

NOMENCLATURE

f	Oscillation frequency
G	Shear modulus
r	Radial position in the cylinder
R	Radius of the cylindrical container
t	Elapsed time
t_{rec}	Recovery time
T_0	Temperature of test fluid
u_ξ	Velocity component along the measurement line
u_θ	Azimuthal velocity component
U_{wall}	Azimuthal velocity on the oscillating wall
Δy	Horizontal displacement of transducer
Θ	Oscillation angle
μ	Viscosity
ν	Kinematic viscosity
ξ	Distance from the transducer
τ	Shear stress
τ_{max}	Maximum shear stress
τ_{Y}	Yield stress
ϕ	Phase lag of the velocity fluctuations
ω	Angular velocity

References

[1] Nicodemo, L., L. Nicolais, and R. F. Landel, "Shear rate dependent viscosity of suspensions in Newtonian and non-Newtonian liquids," Chem. Eng. Sci. **29**, 729–735 (1974).

[2] Dimitriou, C. J., L. Casanellas, T. J. Ober, and G. H. Mckinley, "Rheo-PIV of a shear-banding wormlike micellar solution under large amplitude oscillatory shear," Rheol. Acta. **51**, 395–411 (2012).

[3] Wolthers, W., M. H. G. Duits, D. Van Den Ende, and J. Mellema, "Shear history dependence of the viscosity of aggregated colloidal dispersions," J. Rheol. **40**, 799–811 (1996).

[4] Ancey, C., "Solving the Couette inverse problem using a wavelet-vaguelette decomposition," J. Rheol. **49**, 441–460 (2005).

[5] Yeow, Y. L., W. C. Ko, and P. P. Tang, "Solving the inverse problem of Couette viscometry by Tikhonov regulation," J. Rheol. **44**, 1335–1351 (2000).

[6] Heirman, G., R. Hendrickx, L. Vandewalle, D. Van Gemert, D. Feys, G. De Schutter, B. Desmet, and J. Vantomme, "Integration approach of the Couette inverse problem of powder type self-compacting concrete in a wide-gap concentric cylinder rheometer," J. Non-Newtonian Fluid Mech. **150**, 93–103 (2008).

[7] Stickel, J. J., and R. L. Powell, "Fluid mechanics and rheology of dense suspensions," Ann. Rev. Fluid Mech. **37**, 129–149 (2005).

[8] Doi, M., and T. Ohta, "Dynamics and rheology of complex interfaces," J. Chem. Phys. **95**, 1242–1247 (1991).

[9] *Ultrasonic Doppler Velocity Profiler for Fluid Flow*, Springer Science, edited by Y. Takeda (Springer, Tokyo, 2012).

[10] Gurung, A., J. W. Haverkort, S. Drost, B. Norder, J. Westerweel, and C. Poelma, "Ultrasound image velocimetry for rheological measurements," Meas. Sci. Technol. **27**, 094008 (2016).

[11] Ovarlez, G., F. Bertrand, and S. Rodts, "Local determination of the constitutive law of a dense suspension of noncolloidal particles through magnetic resonance imaging," J. Rheol. **50**, 259–292 (2006).

[12] Jarny, S., N. Roussel, S. Rodts, F. Bertrand, R. Le Roy, and P. Coussot, "Rheological behavior of cement pastes from MRI velocimetry," Cement Concrete Res. **35**, 1873–1881 (2005).

[13] Rodrigez-Gonzalez, F., J. Perez-Gonzalez, L. De Vargas, and B. M. Marin-Santibane, "Rheo-PIV analysis of the slip flow of a metallocene linear low density polyethylene melt," Rheol. Acta **49**, 145–154 (2010).

[14] Perez-Gonzalez, J., J. J. Lopez-Duran, B. M. Marin-Santibanez, and F. Rodriguez-Gonzalez, "Rheo-PIV of a yield-stress fluid in a capillary with slip at the wall," Rheol. Acta **51**, 937–946 (2012).

[15] Quinzani, L. M., R. C. Armstrong, and R. A. Brown, "Use of coupled birefringence and LDV studies of flow through a planar contraction to test constitutive equations for concentrated polymer solutions," J. Rheol. **39**, 1201–1228 (1995).

[16] Rothstein, J. P., and H. M. Gareth, "Inhomogeneous transient uniaxial extensional rheometry," J. Rheol. **46**, 1419–1443 (2002).

[17] Gallot, T., C. Perge, V. Grenard, M. A. Fardin, N. Taberlet, and S. Manneville, Rev. Sci. Instrum. **84**, 045107 (2013).

[18] Ouriev, B., and E. J. Windhab, "Rheological study of concentrated suspensions in pressure-driven shear flow using novel in-line ultrasound Doppler method," Exp. Fluids **32**, 204–211 (2002).

[19] Derakhshandeh, B., D. Viassopoulos, and S. G. Hatzikiriako, "Thixotropy, yielding and ultrasonic Doppler velocimetry in pulp fibre suspensions," Rheol. Acta **51**, 201–214 (2012).

[20] Tasaka, Y., T. Kimura, and Y. Murai, "Estimating the effective viscosity of bubble suspensions in oscillatory shear flows by means of ultrasonic spinning rheometry," Exp. Fluids **56**, 1867 (2015).

[21] Shiratori, T., Y. Tasaka, Y. Oishi, and Y. Murai, "Ultrasonic velocity profiling rheometry based on a widened circular Couette flow," Meas. Sci. Thechnol. **26**, 085302 (2015).

[22] Shiratori, T., Y. Tasaka, and Y. Murai, "Rapid rheological characterization of viscoelastic fluid based on spatiotemporal flow velocimetry," Exp. Therm. Fluids Sci. **71**, 1–13 (2016).

[23] Shiratori, T., Y. Tasaka, Y. Murai, and Y. Takeda, "Development of ultrasonic visualizer for capturing the characteristics of viscoelastic fluids," J. Vis. **16**, 275–286 (2013).

[24] Barnes, H. A., "Thixotropy—A review," J. Non-Newtonian fluids Mech. **70**, 1–33 (1997).

[25] Goh, R., Y.-K. Leong, and B. Lehane, "Bentonite slurries - zeta potential, yield stress, adsorbed additive and time-dependent behaviour," Rheol. Acta **50**, 29–38 (2011).

[26] Lagaly, G., and S. Ziesmer, "Colloid chemistry of clay minerals: The coagulation of montmorillonite dispersions," Adv. Colloid Interface Sci. **100**, 105–128 (2003).

[27] Kelessidis, V. C., and R. Maglione, "Yield stress of water-bentonite dispersions," Colloids Surf. A: Physicochem. Eng. **318**, 217–226 (2008).

[28] Fu, J. T., and M. A. Rao, "Rheology and structure development during gelation of low-methoxyl pectin gels: The effect of sucrose," Food Hydrocolloid **15**, 93–100 (2001).

[29] Suzuki, K., T. Yoneda, and H. Enoto, "Factors affecting to the viscosity of montmorillonite/water suspension," Clay Sci. **50**, 162–174 (2012).

[30] Achenbach, J., *Wave Propagation in Elastic Solids* (Elsevier, Amsterdam, 2012).

[31] Rand, B., E. Pekenc, J. W. Goodwin, and R. W. Smith, "Investigation into the existence of edge-face coagulated structures in Na-montmorillonite suspensions," J. Chem. Soc., Faraday Trans. 1 **76**, 225–235 (1980).

[32] Poelma, C., "Ultrasound imaging velocimetry: A review," Exp. Fluids **58**, 3 (2017).

[33] Meacci, V., S. Ricci, J. Wiklund, B. Birkhofer, and R. Kotzé, "Flow-Viz—An integrated digital in-line fluid characterization system for industrial applications," in *IEEE Sensors Applications Symposium (SAS)* (2016), pp. 1–6.

[34] Fischer, S., P. Schmitt, D. Ensminger, F. Abda, and A. Pallares, "A new velocity estimation method using spectral identification of noise," Flow Meas. Instrum. **19**, 197–203 (2008).